International Journal of Science and Research Archive
eISSN: 2582-8185
Cross Ref DOI: 10.30574/ijsra
Journal homepage: https://ijsra.net/

(RESEARCH ARTICLE)

Check for updates

Biological, Catalytic and *Insilico* Anticancer Activities of Asymmetric Schiff Base and Metal Complexes Derived from Diethylenetriamine, Vanillin and Furfural

Idongesit Nathaniel Ufot *, Nzikahyel Simon and Atim Sunday Johnson

Department of Chemistry, University of Uyo, Uyo, P.M.B 1017, Nigeria.

International Journal of Science and Research Archive, 2026, 20(01), 023-040

Publication history: Received on 22 May 2026; revised on 29 June 2026; accepted on 02 July 2026

Article DOI: https://doi.org/10.30574/ijsra.2026.20.1.1410

Abstract

Antimicrobial resistance (AMR) is a global health emergency requiring innovative discovery strategies. In this work, combinatorial chemistry was employed to synthesise an asymmetric Schiff base, DVF, from diethylenetriamine, vanillin, and furfural, followed by the preparation of Mn(II), Fe(III), and Cu(II) complexes. The products were characterized using conductivity, CHNS analysis, UV-Vis, FTIR, NMR, and XRD spectroscopy. Antimicrobial screening revealed DVF as the most active antibacterial agent compared to the precursors, while the mixed ligand complex - $[Cu(DVF)(S)]_2NO_3$ exhibited superior inhibition against *Staphylococcus aureus* (41 ± 1.2 mm at 500 mg/ml), surpassing chloramphenicol. DVF lacked antifungal activity, but metal coordination enhanced its spectrum. Catalytic studies demonstrated efficient methylene blue degradation, with Fe(III) and Cu(II) complexes achieving >90% removal within 20 minutes under pseudo-first-order kinetics ($R^2 > 0.98$). Molecular docking against breast, prostate, and cervical cancer targets revealed favourable binding interactions, with DVF and its complexes surpassing Tamoxifen and Zometa. The Fe(III) complex (–6.5 kcal/mol) and binuclear Cu(II) complex (–7.6 kcal/mol) showed the strongest affinities, involving hydrogen bonding and π–π stacking, suggesting mechanisms of DNA intercalation, ROS generation, and apoptosis induction. Collectively, DVF and its metal complexes emerged as multifunctional scaffolds with dual biomedical and environmental applications.

Keywords: Diethylenetriamine; Schiff-Bases; Antimicrobial-Drug-Resistance; Cancer; Molecular Docking

1. Introduction

Antimicrobial resistance (AMR) threatens modern medicine by undermining the efficacy of common antibiotics thereby contributing to high morbidity and mortality worldwide. Global analyses estimated that AMR was associated with nearly 5million deaths in 2019 alone, with approximately 1.27 million deaths directly attributable to resistant microbial infections [1, 2]. Although several mechanisms have been proposed for increased AMR prevalence amongst which are; enzymatic drug degradation (example β-lactamases), active efflux, target modification, reduced permeability, and biofilm formation [3]. Mimicking drugs mechanism and genetic mutation are also some of the easiest strategies adopted by these organisms in making potent drugs ineffective within few years of application. Drug classes most affected are β-lactams, fluoroquinolones, aminoglycosides, and macrolides [4]. The WHO priority pathogen list highlights *Carbapenem*-resistant *Acinetobacter baumannii, Pseudomonas aeruginosa*, and *Enterobacteriaceae* (including *Klebsiella pneumonia* and *Escherichia coli*), as well as Methicillin-resistant *Staphylococcus aureus* (MRSA) and Vancomycin-resistant *Enterococcus faecium* [5]. In addition, cancer is now a major public health concern especially in sub-Saharan Africa, being among the three leading causes of premature death in almost all the countries in the region [6]. Among the various types of cancer, prostate, cervical and breast cancer are the most common. Metal complexes of Schiff bases have been reported to exhibit strong catalytic activity, particularly in organic transformations and green chemistry applications [7, 8].

* Corresponding author: Idongesit Nathaniel Ufot

In our earlier studies, we had reported the derivatisation of drugs compounds as one of the strategies in combating this menace [9]. However, the combination of several smaller active organic compounds into a single molecule using condensation reactions as applied in Schiff base formation is a promising methodology.

Combinational chemistry also referred to as combinatorial chemistry is a powerful synthetic approach that enables the rapid generation of diverse chemical libraries by systematically combining multiple building blocks [10]. It accelerates the discovery of new chemical entities by producing diverse libraries of related compounds for high-throughput screening [11]. Schiff bases are compounds formed by condensation of primary amines with aldehydes to give azomethine (–C=N–) linkages. There are particularly amenable to combinational approaches because of facile synthesis and broad structural tunability [12]. Diethylenetriamine like other polyamine offers these characteristics which enables many different aldehydes to be coupled at the different ends of the amine group on its structure [10]. It is a flexible tridentate ligand with two primary amine functionalities that readily condense with aldehydes to form mono-, di-, or tri-Schiff base derivatives depending on stoichiometry and reaction conditions. The resulting azomethine linkages confer planarity and electron delocalization, and the remaining amine or donor sites permit metal coordination—features that influence biological activity and target binding [13]. The aldehydes employed in this work are salicylaldehyde (S) - an ortho-hydroxybenzaldehyde which forms chelating Schiff bases with enhanced stability and potential antioxidant/antimicrobial activity [14], vanillin (V) - a 4-hydroxy-3-methoxybenzaldehyde which can contributes phenolic character and lipophilicity, with reported antimicrobial and anti-inflammatory effects [15], and furfural (F) - a furan-based aldehyde derived from biomass; which introduces heteroaromatic character and has been used in bioactive Schiff base synthesis [16]. Combining these aldehydes with DETA yields asymmetric Schiff base that possess mixed aromatic/heteroaromatic substituents, enabling fine-tuning of lipophilicity, hydrogen-bonding capacity, and electronic distribution parameters that influence membrane permeability and enzyme binding [17, 18].

Hence, in this work, we report asymmetric Schiff base and metal complexes derived from DETA in combination with vanillin and furfural as promising leads in the search for agents that can circumvent AMR, cancer, and as well serve as catalysts.

2. Materials and Methods

All the chemicals were of analytical grades and we used without further purification. The FTIR spectra were recorded on a Shimadzu instrument in anhydrous KBr pellets in the range of 4000-400 cm^{-1}. A Uv-Vis 2500 spectrometer was used to obtain electronic spectra in DMF solutions. The molar conductivities were measured using Hanna conductivity meter. Analysis of elements (CHNS) was carried out using elemental analyser Perkin Elmer series 11 CHNS/O Analyser 2400. The ^{1}H and ^{13}C NMR analyses of the compounds will measured in DMSO solvent using Burker DPX-200 equipment. Powdered XRD analysis was conducted on a Goniometer MiniFlex 300/600 equipment.

2.1. Synthesis of asymmetric Schiff base- DVF

The synthesis of the asymmetric Schiff base of DETA involving vanillin (V) and furfural (F) followed a two steps one-pot method reported in literature [18] and is presented in Figure 1. Some modifications such as adjustment of temperature and pH were adopted where necessary. In the first step, 0.53 cm^3 (5 mmol) of DETA was mixed in 10 cm^3 ethanol in a round bottom flask and stirred at 30 ^{o}C. Then 0.405 cm^3 (5 mmol) furfural (F) mixed in 10 cm^3 of ethanol in a beaker, was added to the round bottom flask and stirred for 30 min to afford a mono-substituted Schiff base. In the second step, 0.753 g (5 mmol) of vanillin (V) dissolved in a 10 cm^3 ethanol was added drop-wise to the mixture of the mono-substituted Schiff base and stirred, 3 some drops of acetic acid was added to maintain the pH between 7 and 8. The reaction mixture was stirred for 2.30 h. The resultant solution was allowed to cooled and evaporate for some days. The resultant black coloured powdered asymmetric Schiff base product was washed with acetone and dried in a desiccator for 48 h. Yield: 78%, MP: >120 ^{0}C, Uv-Vis: λmax, 250 nm, 267 nm (n-n*). FTIR (KBr): cm^{-1}, 3422 (vO-H, vN-H), 2944 (vC-H), 1651 (vC=N), ^{1}H-NMR (DMSOd6) δ: 8.46 (d, J = 8.0Hz, 1H), 8.17 -7.03(mm, 2H), 6.54 (d,J = 4.4Hz,1H), 3.43(s,7H). ^{13}C NMR (DMSO-d6) δ: 169.54(VC=N, 1C, s), 140.56(FC=N, 1C, s), 42.78, 43.23, 42.34 (DETA carbons, 4C, m), Elemental calculated (found) %: C; 64.29(64.74), H; 6. 32(6.71), N; 13.28(13.32).

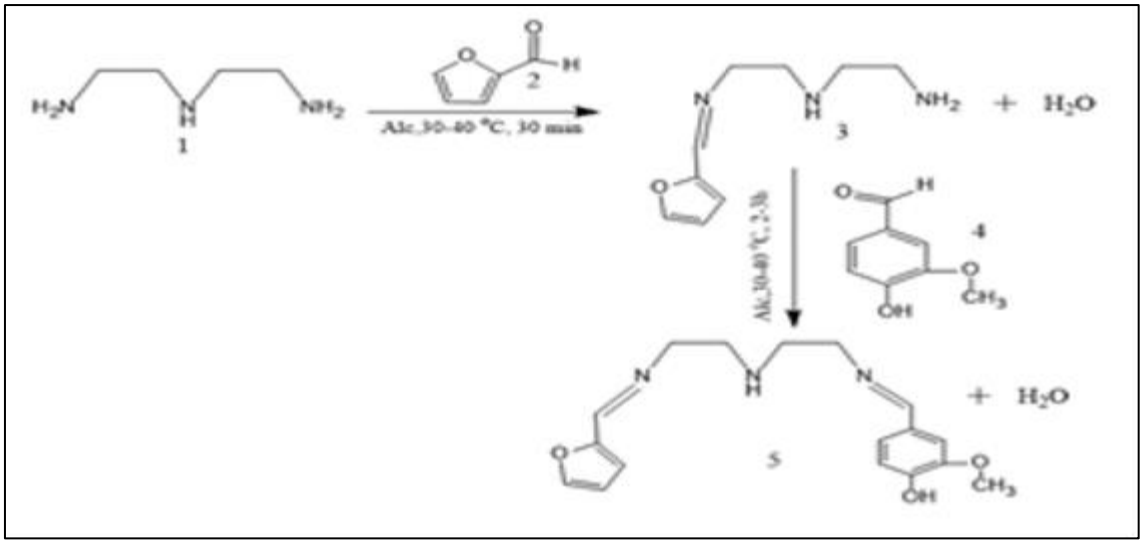

1 = DETA, 2 = Furfural, 3 = Mono condensed Schiff Base, 4 = Vanillin, 5 = 4-[(Z)-({2-[(2-{[(E)-furan-2-ylmethylidene]amino}ethyl)amino]ethyl}imino)methyl]-2-methoxyphenol (DVF).

Figure 1 Schematic representation of the synthesis of asymmetric Schiff bases of DETA

2.2. Synthesis of Cu complex of DVF and Salicylaldehyde (S)

The same procedure was employed for the synthesis of the asymmetric Schiff base as described in Figure 1. However, the metal salts [5 mmol, 1.21 g $Cu(NO_3)_2.3H_2O$)] dissolved in 20 cm^3 of ethanol was added in situ, after stirring for 10 min under reflux in a two necked round bottom flask, 0.525 cm^3 (5 mmol) of S dissolved in 10 cm^3 ethanol was added and reflux for 3 h. The resultant dark brown precipitate was allowed to cooled, then filtered and washed several times in appropriate solvent and dried in a desiccator for further investigation as shown in Figure 2. Yield: 83%, MP: >200 ^oC, Molar Conductivity ($\mu Sm^{-1}cm^{-1}$): 92.60, BM: 1.8, Uv-Vis: λmax, 250, 286 (n-n*), 317 (LMCT). FTIR (KBr): cm^{-1}, 3433 (vO-H, vN-H), 2944 vC-H), 1732 (vC=O) 1632, 1601 (vC=N), 671, 617 (vM-O), 513 (vM-N). ^{1}H-NMR (DMSOd6) δ: 8.54 (s, 1H), 7.58 – 7.52 (m, 1H), 7.50 – 7.46 (m, 1H), 7.35 – 7.25 (m, 2H), 7.06 (d, J = 2.4 Hz, 1H), 6.93 (s, 1H), 6.86 – 6.74 (m, 4H), 3.85 (s, 4H), ^{13}C NMR (DMSO-d6) δ: 162.78, 152.66, 151.56, 148.18, 145.63, 140.30, 137.57, 132.63, 130.79, 127.24, 125.28, 125.19, 122.47, 121.91, 117.10, 113.80, 112.97, 112.03, 110.97, 58.28, 58.05, 56.26, 49.91, 49.86. (DETA carbons, 4C, m), Elemental calculated (found) %: C; 47.56(47.06), H; 4.95(4.42), N; 9.86(10.98), Cu: 10.26(9.96).

2.3. Synthesis of Binuclear Fe (III) Complexes of DVF

The same procedure was employed for the synthesis of the asymmetric Schiff base as described in Figure 1. However, due to difficulty in isolation of the product, 10 mmol (2.70 g) $FeCl_3.6H_2O$ dissolved in 20 cm^3 of ethanol was added in situ, after stirring for 10 min under reflux in a two necked round bottom flask, and reflux for 3 h. Stoichiometry was 2:2. The resultant black paste was allowed to cooled, then filtered and washed several times in diethyl ether and left several days for the solvents to evaporate before being used for further investigation as shown in Figure 2. MP: >150 ^oC, Molar Conductivity ($\mu Sm^{-1}cm^{-1}$): 39.76, BM: 5.2, Uv-Vis: λmax, 271 (n-n*), 394 (LCMT). FTIR (KBr): cm^{-1}, 3395 (vO-H, vN-H), 2943 vC-H), 1624, 1589 (vC=N), 687, 637 (vM-O), 484, 455 (vM-N). ^{1}H-NMR (DMSOd6) δ: 10.41 (d, J = 4.4 Hz, 1H), 9.68 (d, J = 1.4 Hz, 1H), 7.29 (d, J = 1.4 Hz, 1H), 5.16 (d, J = 4.4 Hz, 1H), 4.85 (s, 1H), 4.66 (s, 1H), 3.30 (s, 5H), 2.39 (s, 27H). ^{13}C NMR (DMSO-d6) δ: 152.26, 152.23, 151.65, 151.56, 148.23, 148.18, 145.66, 145.63, 140.76, 129.62, 129.59, 124.96, 113.82, 113.80, 113.05, 113.03, 112.04, 112.03, 111.25, 111.24, 56.29, 56.26, 51.79. (DETA carbons, 4C, m), Elemental calculated (found) %: C; 47.47(47.97), H; 5.47(5.08), N; 11.26(11.76), Cu: 13.36(13.61).

2.4. Synthesis of Mn complex of DVF and citric acid (CA)

The same procedure was employed for the synthesis of the asymmetric Schiff base as described in earlier. Then, 5 mmol of the metal salts [1.49 g $MnCl_2.2H_2O$] dissolved in 20 cm^3 of ethanol was added in situ, after stirring for 10 min under reflux in a two necked round bottom flask, 5 mmol of CA (0.0961 g) dissolved in 10 cm^3 ethanol and deprotonated with 3 M NaOH was added in drops slowly. The mixture was refluxed for 3 h. The resultant precipitate was allowed to cooled, then filtered and washed several times in diethyl ether, rinsed with cold ethanol and dried in a desiccator for further investigation as shown. The reaction is simplified in Figure 2. Yield: 63%, MP: >190 ^oC, Molar Conductivity ($\mu Sm^{-1}cm^{-1}$): 97.90, BM: 5.7, Uv-Vis: λmax, 250 (n-n*), 366 (LMCT), 479 (d-d). FTIR (KBr): cm^{-1}, 3295 (vO-H, vN-H), 2847 vC-H), 1636, 1582 (vC=N), 1366 v(NO_3^-), 679, 629 (vM-O), 579, 544, 471 (vM-N). ^{1}H-NMR (DMSOd6) δ: 8.09 – 8.05 (m, 2H), 7.71 – 7.63 (m, 3H), 7.36 – 7.32 (m, 2H), 7.18 (dd, J = 8.6, 2.3 Hz, 1H), 7.12 (d, J = 2.4 Hz, 1H), 6.87 – 6.79 (m, 2H), 6.77 – 6.72

(m, 1H), 3.86 (s, 4H), 3.34 – 3.25 (m, 7H), 3.21 (s, 1H), 3.19 – 3.12 (m, 4H), 3.05 (dd, J = 8.5, 6.7 Hz, 2H), 3.00 – 2.93 (m, 4H), 2.92 (s, 1H). ^{13}C NMR (DMSO-d6) δ: 175.33, 169.36, 152.27, 151.56, 148.18, 145.63, 141.62, 130.40, 125.62, 122.61, 113.80, 112.94, 112.03, 111.16, 75.08, 58.11, 56.26, 49.17, 49.09, 49.02, 46.37, 41.27, 41.20, 41.12. Elemental calculated (found) %: C; 43.90(43.48), H; 4.00(3.69), N; 6.68(6.66), Mn: 8.73(8.65).

2.5. Synthesis of Binuclear Cu (II) Complex of DVF

The same procedure was employed for the synthesis of the asymmetric Schiff base as described earlier. A 2:2 stoichiometry was adopted. The metal salts [10 mmol, 2.42 g $Cu(NO_3)_2.3H_2O$] dissolved in 20 cm^3 of ethanol was added in situ, it was stirred under reflux in a two necked round bottom flask for 3 h. The resultant precipitate was allowed to cooled, then filtered and washed several times in methanol and rinse with ether and dried in a desiccator for further investigation [19]. The mechanism of this reaction is illustrated in Figure 2. Yield: 80%, MP: >199 ^{o}C, Molar Conductivity (μSm^{-1}cm^{-1}): 18.08, BM: 1.98, Uv-Vis: λmax, 250 (n-n*), 596.2 (d-d). FTIR (KBr): cm^{-1}, 3433 (vO-H, vN-H), 2248 vC-H), 1636, 1601 (vC=N), 1385 (vNO_3^-), 671, 590, 625 (vM-O), 459 (vM-N). ^{1}H-NMR (DMSOd6) δ: δ 8.09 (d, J = 25.5 Hz, 1H), 7.67 (d, J = 18.3 Hz, 1H), 7.21 – 7.06 (m, 1H), 6.80 (dd, J = 51.6, 7.5 Hz, 1H), 3.96 (s, 2H), 3.27 – 2.86 (m, 1H)., ^{13}C NMR (DMSO-d6) δ: 152.76, 152.71, 151.56, 148.18, 145.62, 140.82, 130.13, 125.48, 122.46, 113.83, 113.01, 111.38, 110.96, 56.29, 53.64, 49.33. Elemental calculated (found) %: C; 43.47(43.73), H; 4.89(4.91), N; 11.94(12.00), Cu: 13.56(13.61).

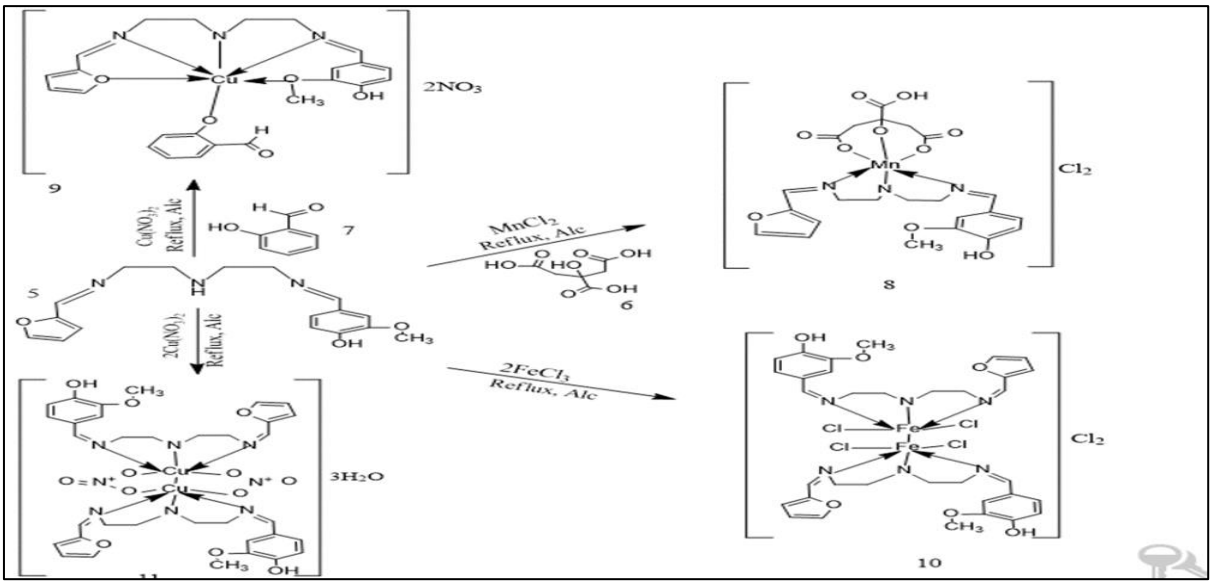

5 = DVF, 6 = Citric acid, 7 = Salicylaldehyde, 8 = $[Mn(DVF)(CA)]Cl_2$, 9 = $[Cu(DVF)(S)]2NO_3$, 10 = $[Fe_2(DVF)_2(Cl)_4]Cl_2$, 11 = $[Cu_2(DVF)_2(NO_3)_2]3H_2O$

Figure 2 Schematic representation of the synthesis of metal complexes of DVF Schiff base showing their proposed structures

3. Antimicrobial Studies

The antimicrobial studies conducted involved selected bacteria and fungi. The activities of the synthesised Schiff bases were determined using the method reported in the literatures [20, 21]. A seeded nutrient agar on which 0.5-mm-diameter wells were punched was used. Different concentrations 100 mg/cm^3 to 500 mg/cm^3 of sterile filtered solutions of the compounds were made using DMSO as solvent, Chloramphenicol and Nystatin as control for bacteria and fungi respectively. 0.1 cm^3 of each concentration was applied to the wells and incubated at 37 ^{o}C for two days for bacteria, and 28 ^{o}C for 72 h for fungal isolates. The antimicrobial activity of the compounds was estimated on the basis of the size of the zone of inhibition around the wells on the seeded nutrient agar. The bacteria species used were *Staphylococcus aureus*, *Escherichia coli*, *Streptococcus pneumonia* and *Pseudomonas aeruginosa* while the fungi species included *Aspergillus niger* and *Can*dida *albicans*. The percentage inhibition was calculated using the formula:

$$\% \text{ Inhibition} = [(A-B)/A] \times 100 \quad - \quad - \quad - \quad (1)$$

where A = diameter of the organism growth in the control

B = diameter of the organism growth in the test plate.

4. Catalytic Studies

The catalytic evaluations of the tested compounds were based on the method reported by Zhang *et al*. (2019) [22] and Fasna *et al*. (2022) [23] with some modifications. The method evaluated the ability of the compounds to degrade methylene blue (MB) in the presence of hydrogen peroxide (H_2O_2). In the first step, 0.0159 g of MB was completely dissolved in 50 cm^3 deionized water in the dark. In another 200 cm^3 beaker, 2 % H_2O_2 was prepared under the same condition. Then, the various compounds to be tested were prepared by dissolving 1 mg each in 10 cm^3 DMSO in separate beakers. In the second step, to a calibrated Uv-Vis spectrophotometer, with wavelength set at 652 nm and 4 min reading interval for 20 mins duration, 6 cm^3 of the prepared MB was mixed properly with 4 cm^3 of the H_2O_2 and quickly turn into the cuvette for readings at every 4 min interval,

Lastly, 6 cm^3 MB (prepared) plus 4 cm^3 H_2O_2 was added quickly to 2 cm^3 DMSO and mixed properly. Then readings were taken as before. After that, 6 cm^3 of the prepared MB plus 4 cm^3 H_2O_2 was mixed quickly to 2 cm^3 of the dissolved samples and absorbance recorded. Degradation Efficiency (D %) was calculated using equation 2 at time t with various samples in the presence of H_2O_2 (10^{-2} M). C0 and Ct are the MB concentrations at time 0 and t respectively. The rate equation fitted equation 3.

$$\mathbf{D}\% = [(\mathbf{C0} - \mathbf{Ct})/\mathbf{C0}] \text{ x } 100 \quad - \quad - \quad - \quad (2)$$

$$\mathbf{ln}\left[\frac{\mathbf{C0}}{\mathbf{Ct}}\right] = \boldsymbol{kt} \quad - \quad - \quad - \quad - \quad - \quad - \quad (3)$$

where k = the rate constant, t = time

5. *Insilico* Evaluation of Interactions of the Asymmetric Schiff Base and the Metal Complexes in Cancer Cells Using Molecular Docking

5.1. Ligands and Target Macromolecules Preparation

In this study, the Pyrx software (version 0.9.8), embedded with Autodock Vina tools was used for the docking process because of its simplicity and accuracy [24]. The ligands (Schiff bases) were drawn using Chemsketch (Freeware 2023.1.1) and converted to the desired structure data format (sdf) using of Open babel program. The target protein molecules were downloaded as 3D structures from Protein Data Bank (PDB) website [25] and saved in PDB format. Discovery studio was used to visualise and prepare the target proteins by deleting water molecules, ligands present and all other chains except one to avoid complexity in the process [26]. After these, polar hydrogen was introduced to the target molecule before being saved in PDB format.

5.2. Docking Protocols

In the docking procedures, the target protein was opened in the PyRx and converted to pdbqt format. Then, the ligands were loaded using the open babel program embedded in PyRx, their energy minimised based on the default Autodock Vina force field, and then, were converted to pdbqt format before running the Autodock Vina program embedded in the PyRx software. The grid box centers and dimensions were set at maximum and hence generated automatically by the program to cover the entire surface of the target protein [27].

The investigated macromolecule were cervical cancer -1A7G (transcription regulatory protein E2)[28], breast cancer – 1WYX (cell adhesion protein) [29] and prostate cancer – 2OZ7 (hormone receptor protein) [30].

6. Results and Discussion

6.1. Physical Properties of the Ligand and Complexes

The asymmetric Schiff base (DVF) and its metal complexes exhibited distinct physical properties which indicate successful synthesis. DVF appeared as a black powdered solid which is soluble in DMSO and DMF, and slightly soluble in alcohols. Hence, the metal complexes were synthesised *insitu* after each round of preparation. It shows a melting point above 120 °C, while its metal complexes showed higher decomposition points (>190–200 °C), reflecting enhanced thermal stability due to strong metal–ligand interactions. Also, among the complexes, $[Cu_2(DVF)_2(NO_3)_2]3H_2O$ is insoluble in alcohol while the rest are slightly soluble. Molar conductivity values ranged from 18.08 to 97.90 $\mu Sm^{-1}cm^{-1}$, indicating both electrolytic and non-electrolytic behavior of the complexes [31]. Magnetic susceptibility measurements

revealed paramagnetism in Fe(III) (BM ~5.2) and Mn(II) (BM ~5.7) complexes, consistent with high-spin configurations, while Cu(II) complexes showed lower magnetic moments (~1.8–1.98 BM), typical of d^9 systems [32]. Both Cu complexes are paramagnetic because Cu(II) in a d^9 system has one unpaired electron. The mononuclear Cu complex value of 1.8 BM corresponds with the spin-only expected value, while the binuclear Cu complex value of 1.98 BM is slightly higher due to weak ferromagnetic exchange interactions between the two Cu centers (Figure 2). The calculated elemental composition is in good agreement with the found.

6.2. Electronic Spectral Studies

Electronic spectra provided evidence of coordination and electronic transitions. DVF displayed absorption maxima at 250 and 267 nm, attributed to n–π* transitions of the azomethine group. The UV-Vis spectra of the individual reactants (DETA, furfural, and vanillin) compared with the asymmetric Schiff base DVF provide clear evidence of structural transformation and extended conjugation (Figure 3). DETA exhibited a sharp, intense absorption band near 250 nm, characteristic of n– σ* transitions from the lone pair electrons on aliphatic amine nitrogen atoms. This strong peak reflects its simple electronic structure without aromatic conjugation [33]. The observed transitions occurs when electrons absorb energy and move to the higher - energy levels. In this case, it occurred between the nonbonding (n) electrons on the nitrogen atoms moving to the anti-bonding orbitals (σ*). Upon successful condensation, the peak is drastically reduced and shifted due to conjugations from the azomethine couplings and the aromatic systems from the aldehydes (13, 14). Furfural showed smoother absorbance features with moderate intensity, arising from π–π* transitions within the furan ring. Its conjugation is limited, resulting in absorption at slightly longer wavelengths than DETA but with lower overall intensity [34]. Vanillin, in contrast, displayed distinct peaks in the 300–350 nm regions. The phenolic –OH and methoxy substituents extended conjugation and introduced charge-transfer transitions, explaining its stronger absorbance in the near-UV region [35].

Upon Schiff base formation (DVF), the spectrum retains the 250 nm bands and introduces a new absorption at 335 nm, indicative of extended conjugation and azomethine formation ($\pi \rightarrow \pi*$) [36]. The imine (–C=N–) linkage introduced new n–π* transitions, while conjugation between vanillin's aromatic ring and furfural's heteroaromatic system extended electron delocalization. As a result, DVF absorbed over a wider range, with smoother intensity compared to the sharp DETA peak, and showed bathochromic (red-shifted) behavior relative to the reactants. This spectral feature confirms successful condensation [37]. Schiff bases are known to exhibit broader, shifted absorption compared to their parent amines and aldehydes, due to the formation of azomethine linkages and increased planarity [38, 39]. The observed changes confirms DVF as an asymmetric Schiff base with conjugated aromatic rings and imine groups. The extended π-electron delocalization broadens the absorption bands, producing overlapping n → π* and π → π* transitions. This results in smoother, wider absorption bands compared to the sharp localized transition in the starting materials. Thus, the UV-Vis analysis not only validates the structural transformation but also explains the functional improvements in DVF relative to its precursors [40].

The metal complexes exhibited additional ligand-to-metal charge transfer (LMCT) and d–d transitions. For example, Mn(II) complexes showed LMCT absorptions at 366 and 479 nm. While the binuclear Cu(II) complex displayed a prominent d–d band at 596 nm, the mononuclear complex showed a band at 317 nm attributed to LMCT. The d-d transitions in the binuclear complex could be attributed to the effects of the bridging ligands and metal – metal interactions which enhanced ligand field stabilization and reduction of the energy required for a d-d transitions to occur [36]. The binuclear Fe(III) complex displayed a similar ligand –centered transition around 253 and 288 nm, along with a weak band at 394 nm, which is characteristic of a d-d transitions and LMCT in Fe(III) bridged systems [41]. These spectral features confirmed coordination, and an altered electronic environments, enabling redox activity [42].

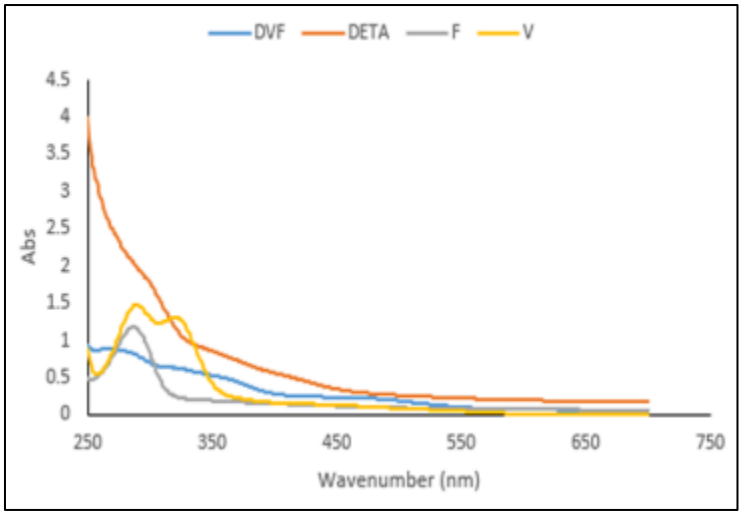

Figure 3 Stacked UV-Vis Spectra of DETA, Furfural (F), Vanillin (V) and DVF

6.3. FTIR Analysis

FTIR spectra revealed characteristic shifts upon complexation (Figure 4). DVF spectrum does not show a band attributable to C=O vibrations in the aldehydes (1680 -1720 cm^{-1}). Rather, it exhibited a strong azomethine (C=N) stretch at ~1651 cm^{-1}, which shifted to lower frequencies (1601–1624 cm^{-1}) in the complexes, indicating condensation and coordination of the imine nitrogen to the metal center [40, 43]. Since, the aldehydes are different, it would be expected to have two distinct azomethine signals as seen in $[Cu(DVF)(S)]2NO_3$, and $[Fe_2(DVF)_2(Cl)_4]Cl_2$, however, due to conjugations that results in extensive peak broadening, these signals are not properly resolved in DVF (Figure 4) and the other complexes. The retention of C–N bands suggests that the secondary DETA nitrogen atoms remained available for coordination, indicating potential donor sites in the ligand [44]. In addition, the appearance of bands between 617–687 cm^{-1} and 459–513 cm^{-1} which correspond to M–O and M–N vibrations, respectively confirms the coordination through DVF nitrogen and oxygen [45]. The presence of hydroxyl and amine stretches around 3400 cm^{-1} indicates residual donor sites available for water coordination and hydrogen bonding [14, 46].

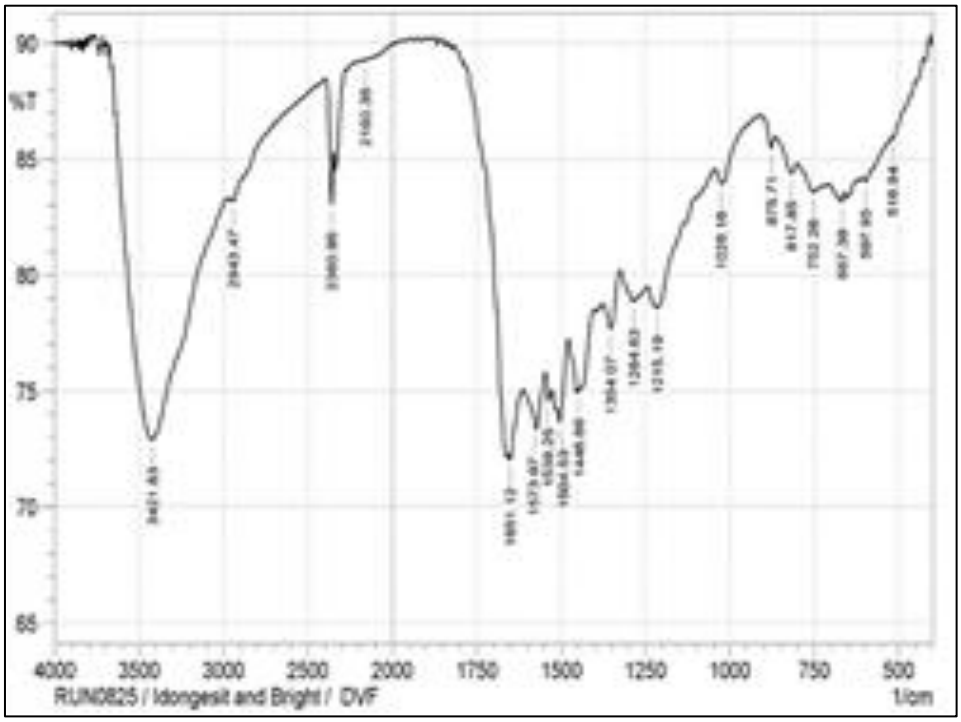

Figure 4 FTIR Spectrum of DVF

6.4. ^{1}H and ^{13}C spectroscopic analysis

^{1}H and ^{13}C NMR spectra of DVF are presented in Figure 5 and 6. This asymmetric Schiff base showed signal for DETA protons (around δ 2.2 -3.43 ppm) as overlapping multiplets reflecting the conformational flexibility of the triamine framework [47], and imine protons from furfural (δ 7.83 ppm) and vanillin (δ 8.52 ppm) in DMSO-d6. The methoxy singlet at δ 3.7–3.9 ppm confirms the presence of vanillin condensed portion [48]. As observed in Figure 5, the imine proton appeared downfield at δ 8.46 ppm, while aromatic protons resonated between δ 7.03–8.17 ppm. The azomethine carbon resonance at δ 150 – 165 ppm is consistent with the reported Schiff base spectroscopic signatures [49]. In complexes, slight shifts in imine and aromatic signals were observed, reflecting deshielding due to coordination. Thus, Cu(II), Mn(II), and Fe(III), complexes showed significant spectral perturbations that confirmed metal binding through the N_2O_2 donor set. The imine proton and carbon signals underwent downfield shifts of Δδ 0.2–0.5 ppm and Δδ 5–15 ppm, respectively, indicating direct coordination of the azomethine nitrogen to the metal center, while the disappearance or dramatic shift of the phenolic –OH signal confirms deprotonations and phenolate oxygen binding [50]. The paramagnetic complexes exhibited characteristic features including extreme chemical shift ranges (δ –50 to +100 ppm for Fe(III)) and severe line broadening, observed with the binuclear Cu(II) and Fe(III) assemblies displaying doubled carbon signals that confirm magnetically inequivalent ligand environments in the dimeric structures [51].

In $[Cu(DVF)(S)]_2NO_3$, the imine proton signal disappears in the ^{1}H NMR spectrum, because the imine nitrogen has coordinated to the metal center. Aromatic signals broaden slightly, reflecting electronic perturbations [52]. In the ^{13}C NMR spectrum, the imine carbon shifted upfield to ~158 ppm as a result of electron donation to the Cu(II) center [53]. For $[Mn(DVF)(CA)]Cl_2$, the imine proton is retained but shifted downfield (~8.6 ppm), which shows a weaker coordination compared to Cu(II). The imine carbon resonates around δ 160 ppm, with additional deshielding of aromatic carbons. This observation supports similar scenario reported by Nakamoto [54]. In $[Cu_2(DVF)_2(NO_3)_2]\cdot 3H_2O$, both imine protons disappeared, and the aromatic region showed pronounced broadening, consistent with multinuclear coordination. The imine carbon shifted further upfield (δ 157 ppm), while quaternary carbons adjacent to donor atoms are deshielded, supporting bidentate coordination through imine nitrogen and phenolic oxygen. Lastly, in $[Fe_2(DVF)_2Cl_4]Cl_2$, the imine proton disappeared completely, and aromatic protons are significantly broadened, due to strong paramagnetic effects of Fe(III). The imine carbon resonance shifted to ~155 ppm, and phenolic carbons are deshielded, suggesting tridentate coordination involving imine nitrogen, phenolic oxygen, and possibly furan oxygen [55].

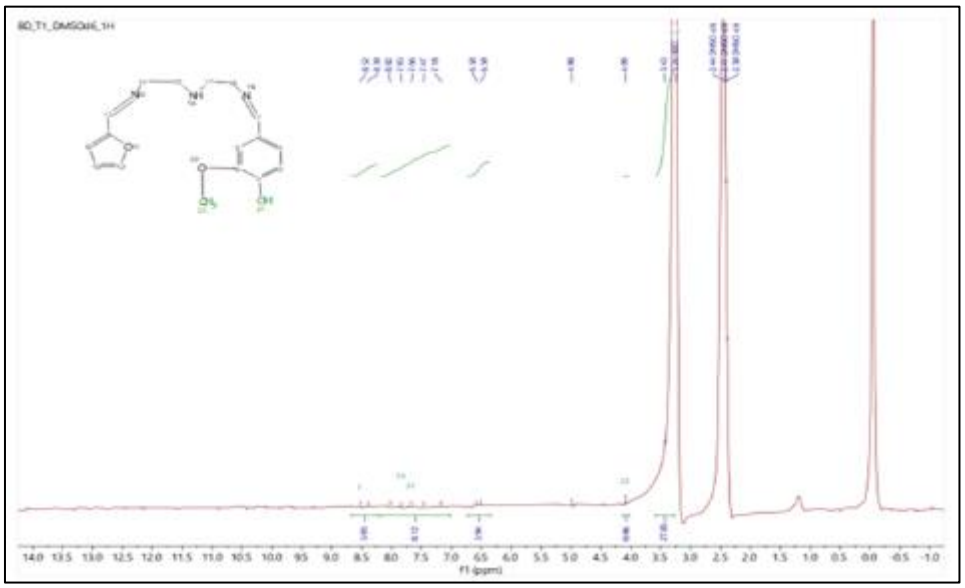

Figure 5 ^{1}H NMR Spectrum of DVF

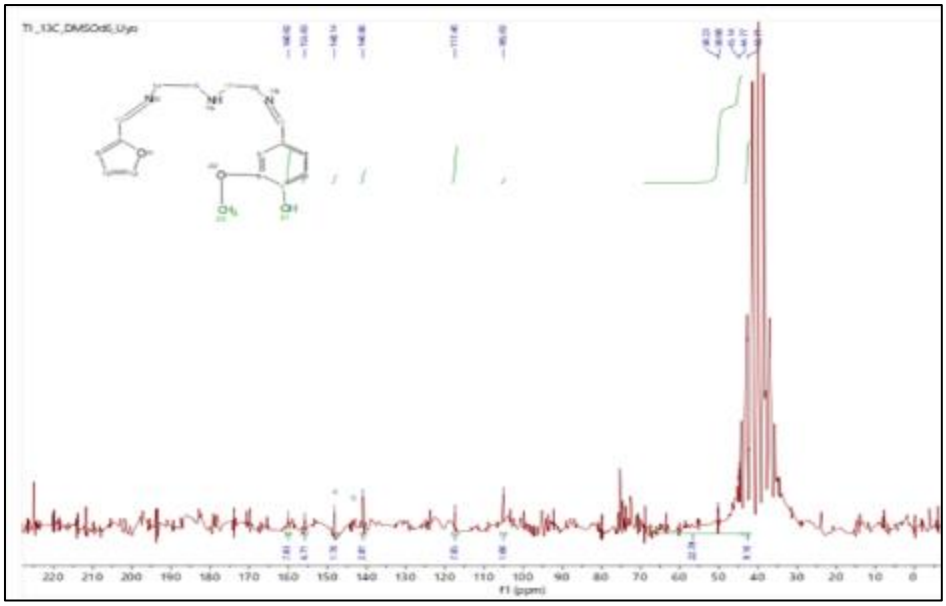

Figure 6 ^{13}C NMR Spectrum of DVF

6.5. XRD Analysis of DVF

The powder XRD patterns of DVF shown in Figure 7 exhibits characteristic features which support successful synthesis of DETA-derived asymmetric Schiff bases as reported in literature [56]. This includes broad amorphous halos (diffuse scattering rings) centered in the 15–25° 2θ range with no sharp diffraction peaks (Figure 7), which is peculiar to polyamine Schiff base materials where condensation between the primary and secondary amine groups of DETA and the carbonyl functionalities of the respective aldehydes generates highly branched, cross-linked imine networks that inherently suppress long-range crystalline order [49, 57]. The broad diffraction halo observed across the compound arises from short-range ordering within the amorphous Schiff base matrix. This pattern also showed an amorphous halo centered near 22°, specifically considering the peaks at 15.5°, 17.3°, and 22.75° (d-spacing 5.72 Å, 5.13 Å, 3.91 Å), corresponding to crystallite sizes of ~3.3–4.1 nm which is a sign of consistent formation of the imine-linked network [58, 59]. The absence of sharp crystalline peaks in the spectrum (Figure 7) further proved that neither unreacted DETA nor free aldehyde precursors remained in the final products. Ordinarily, free ligands such as DETA and aldehydes used in this work are small rigid molecules which should give sharp and well-defined crystalline reflections [59].

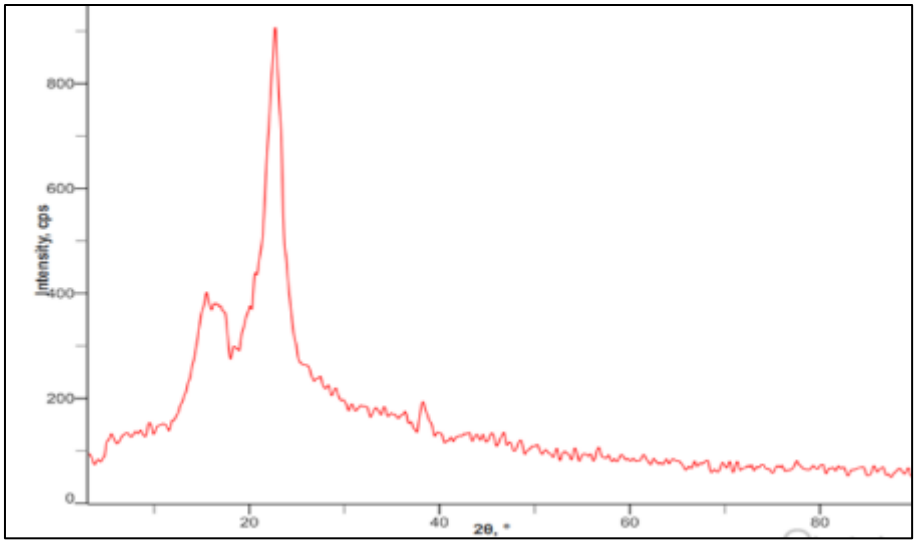

Figure 7 XRD Spectrum of DVF

The amorphous nature of these materials is structurally inherent to DETA-based Schiff bases, as the tridentate amine backbone with three reactive nitrogen centers. This creates a hyper branched polymeric architecture that cannot readily

pack into ordered crystalline lattices [60]. This structural characteristic distinguishes DETA Schiff bases from simpler diamine-derived analogues, which may exhibit greater crystallinity due to their more linear, symmetric structures [50, 61]. Therefore, this XRD data further confirms the successful formation of DVF as DETA-derived asymmetric Schiff base.

6.6. Antibacterial analysis

Antibacterial assays demonstrated broad spectrum activity. DVF and the complexes showed significant antibacterial effects, particularly against *Staphylococcus aureus* and *Streptococcus pneumonia* (Table 1). The mixed ligands Cu(II) complex -$[Cu(DVF)(S)]_2NO_3$, exhibited the highest inhibition against *Staphylococcus aureus* (41 ± 1.2 mm), surpassing chloramphenicol (35 ± 1.2 mm). The Fe(III) complex also showed strong inhibition (38 ± 1.2 mm). These results highlight the role of metal coordination in enhancing activity by increasing lipophilicity and facilitating penetration through bacterial membranes. This observation is consistent with previous findings that metal chelation enhances antimicrobial efficacy [63]. The paramagnetic nature of Fe(III) and Cu(II) complexes supports ROS generation, which damages bacterial proteins and DNA [3]. Gram negative bacteria (*E. coli, P. aeruginosa*) were less susceptible, due to their protective outer membranes [15].

6.7. Antifungal analysis

Antifungal screening revealed moderate inhibition against *Candida albicans*, with $[Fe_2(DVF)_2(Cl)_4]Cl_2$ (24 ± 1.1 mm) and $[Cu(DVF)(S)]_2NO_3$ (18 ± 1.2 mm) outperforming other compounds. Activity against *Aspergillus niger* was weaker (<13 mm), reflecting the resilience of filamentous fungi. Schiff bases containing aromatic substituents and hydroxyl groups enhanced antifungal activity due to improved lipophilicity and hydrogen bonding [39]. Also, as reported by Ali *et al.* 2019 [64], Schiff bases containing imine groups (–C=N–) and aromatic substituents enhance binding to fungal enzymes, disrupting ergostrol biosynthesis in fungal membranes. Transition metals further amplify antifungal activity by facilitating electron transfer reactions that destabilize fungal cell walls, therefore have more activity than the free ligands [32].

6.8. Evaluations of the Binding Affinity and Interactions of the Studied Compounds against Cancer cells

The binding interactions and binding affinities of DVF, its precursors and the metal complexes are presented in Table 2 and in Figure 8 – 10. The docking studies revealed favourable binding affinities for DVF and its complexes against breast (1WYX), cervical (1A7G), and prostate (2OZ7) cancer targets. The parent ligands (DETA, furfural, and vanillin) exhibited relatively weak binding affinities, ranging between –2.7 and –4.2 kcal/mol across breast (1A7G), prostate (2OZ2), and cervical (1WYX) cancer targets. These values are lower than those of standard drugs such as Tamoxifen (–5.0 kcal/mol) and Zometa (–5.2 kcal/mol), indicating that the simple precursors lack strong interactions with cancer cell proteins. This observation is consistent with reports that free aldehydes and amines generally show limited anticancer activity due to insufficient conjugation and weak hydrogen bonding capacity [65]. In contrast, the asymmetric Schiff base DVF demonstrated significantly stronger binding affinities, with values of –5.6, –7.0, and –5.5 kcal/mol across the three cancer targets. The results surpassed that of the control drugs confirming that the combination is a better approach. The effectiveness of DVF could be related to the imine (–C=N–) linkage and extended conjugation which facilitate π–π stacking and hydrogen bonding with active site residues, thereby improving stability within the binding pockets of the macromolecules [25, 66]. The metal complexes showed stronger interactions suggesting potential anticancer activity through apoptosis induction and ROS mediated pathways [27].

The Mn(II) complex $[Mn(DVF)(CA)]Cl_2$ showed moderate binding (–5.1 to –6.4 kcal/mol), while the Cu(II) complex $[Cu(DVF)(S)]_2NO_3$ displayed affinities up to –5.5 kcal/mol, comparable to DVF itself. These results align with findings showing that copper complexes enhance anticancer activity by generating reactive oxygen species (ROS) and promoting apoptosis [67]. The Fe(III) complex $[Fe_2(DVF)_2(Cl)_4]Cl_2$ demonstrated a stronger binding affinity (–6.0 to –6.5 kcal/mol), surpassing Zometa, consistent with reports that Fe(III) complexes stabilised radical intermediates and interacted with DNA grooves [68]. Most notably, the binuclear Cu(II) complex $[Cu_2(DVF)_2(NO_3)_2]\cdot 3H_2O$ exhibited the highest binding affinities (–7.3, –7.6, –5.5 kcal/mol), outperforming all controls. Literature confirms that binuclear copper Schiff bases exhibit superior anticancer activity due to synergistic redox cycling and enhanced DNA intercalation [64]. Additionally, the docking interactions indicate potential binding to kinases and hormone receptors, aligning with reported anticancer pathways in literature [37]

Table 1 Results of Antibacterial and Antifungal analysis

	Zones of Inhibition Diameter (mm)/ Concentration (500 mg/mL)					
Compounds	***Staph A***	***S. pneumonia***	***P. aeruginosa***	***E. coli***	*Candida albicans*	*A. niger*
1	24±1.1	17 ± 1.0	NA	8 ± 1.0	17±1.1	NA
2	NA	NA	13 ± 1.1	15 ± 1.1	NA	NA
4	7±1.0	NA	NA	NA	10 ± 1.0	NA
5	21 ± 1.3	25 ± 1.1	17 ± 1.1	15 ± 1.4	10 ± 1.0	NA
6	29± 1.5	25 ± 1.2	19 ± 1.2	15 ± 1.2	10 ± 1.1	NA
7	15 ± 1.2	19 ± 1.1	10 ± 1.0	15 ± 1.1	14 ± 1.2	10 ± 1.1
8	20 ± 1.0	23 ± 1.1	19 ± 1.2	15 ± 1.2	12 ± 1.0	8 ± 1.0
9	41 ± 1.2	32 ± 1.2	29 ± 1.1	24 ± 1.2	18 ± 1.2	13 ± 1.2
10	38 ± 1.2	32 ± 1.1	32 ± 1.1	30 ± 1.1	24 ± 1.1	13 ± 1.2
11	30 ± 1.1	22 ± 1.1	28 ± 1.2	23 ± 1.0	15 ± 2.1	11 ± 1.3
12 **(20 mg/mL)**	35±1.2	28± 1.0	20 ± 1.3	26 ± 1.1	-	-
13 (30 mg/mL)	-	-	-	-	33± 1.0	16 ± 1.2

1 = DETA, 2 = Furfural, 4 = Vanillin, 5 = DVF, 6 = Citric acid, 7 = Salicylaldehyde, 8 = $[Mn(DVF)(CA)]Cl_2$, 9 = $[Cu(DVF)(S)]2NO_3$, 10 = $[Fe_2(DVF)_2(Cl)_4]Cl_2$, 11 = $[Cu_2(DVF)_2(NO_3)_2]3H_2O$., 12 = Chloramphenicol(Antibacterial control), 13 = Nystatin (Antifungal control), NA = No activity, (-) = Not applicable

Table 2 Molecular Docking Results of the studied compounds on Cancer cells

Compounds	**Binding Affinity (kcal/mol)**		
	1A7G	**2OZ2**	**1WYX**
1	-3.2	-3.1	-3.5
2	-3.8	-4.1	-2.7
4	-4.2	-5.7	-3.7
5	-5.6	-7.0	-5.5
6	-4.2	-5.6	-4.5
7	-4.8	-5.3	-3.5
8	-5.1	-6.4	-4.7
9	-4.9	-5.5	-3.6
10	-6.0	-6.5	-5.1
11	-7.3	-7.6	-5.5
Avastin (control)	-5.6	-	-
Tamoxifen(control)	-	-	-5.0
Zometa (control)	-	-5.2	-

1 = DETA, 2 = Furfural, 4 = Vanillin, 5 = DVF, 6 = Citric acid, 7 = Salicylaldehyde, 8 = $[Mn(DVF)(CA)]Cl_2$, 9 = $[Cu(DVF)(S)]2NO_3$, 10 = $[Fe_2(DVF)_2(Cl)_4]Cl_2$, 11 = $[Cu_2(DVF)_2(NO_3)_2]3H_2O$. 12 = Nystatin, (-) = No applicable

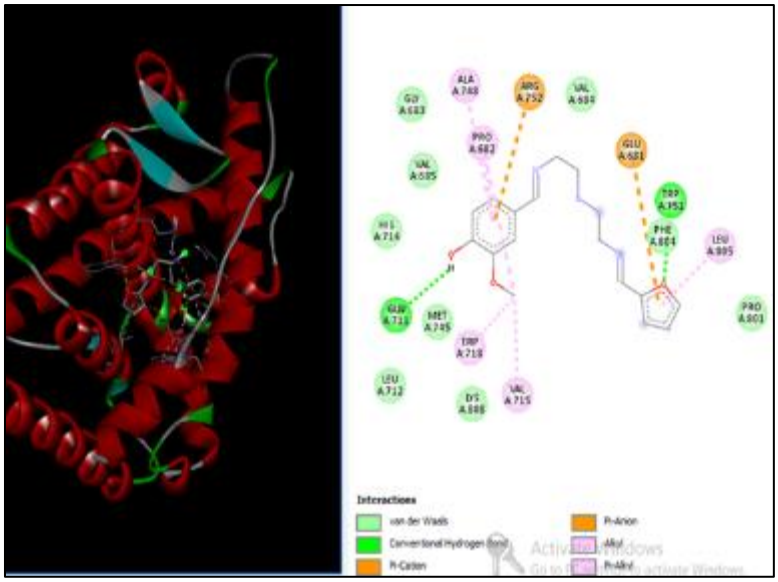

Figure 8 2D and 3D representation of DVF interactions with 2OZ7

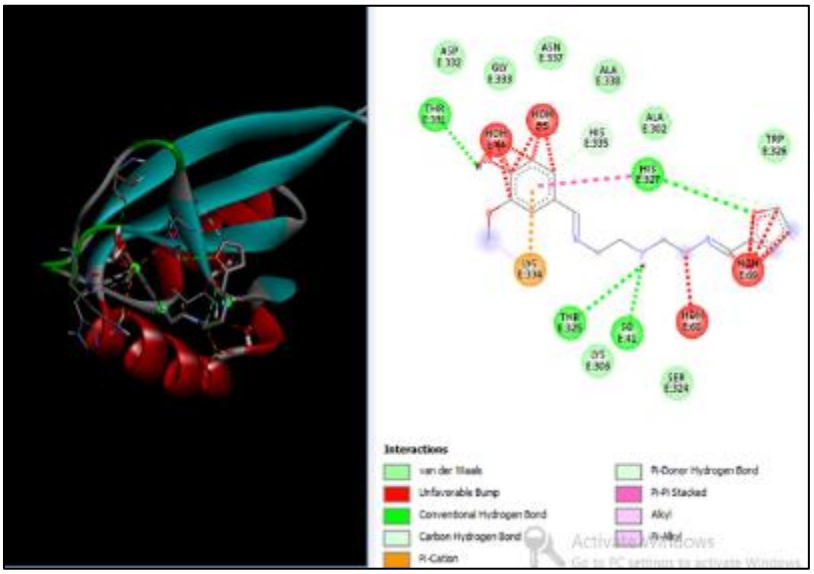

Figure 9 2D and 3D representation of DVF interactions with 1A7G

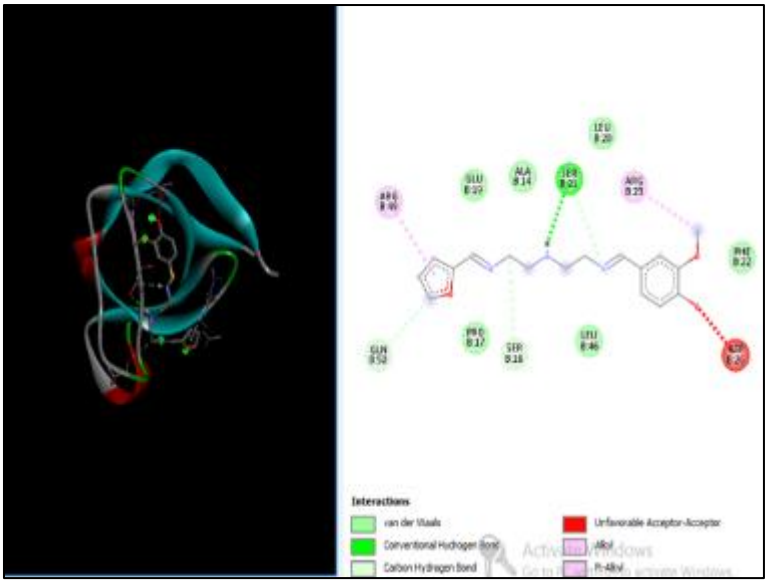

Figure 10 2D and 3D representation of DVF interactions with 1WYZ

6.9. Catalytic Studies

Catalytic degradation of methylene blue followed pseudo-first-order kinetics (R^2 > 0.98). The Fe(III) complex **[**$Fe_2(DVF)_2(Cl)_4]Cl_2$ (k = 0.115 min^{-1}) and Cu(II) complexes showed the highest catalytic efficiency. The mechanism involves MLCT under visible light, generating ROS such as hydroxyl radicals that oxidized MB [41]. These results are in line with previous studies on Schiff base complexes as catalysts for dye degradation [69]. The effectiveness of these complexes can be explained in terms of their structural robustness which is confirmed by their high decomposition point (>200 ^oC) and paramagnetism (BM = 5.2 for Fe complexes), which supports their redox activity and catalytic efficiency. As reported by Fasna *et al*. [23], these complexes can recycle their oxidation states facilitating continuous ROS generation. The catalytic degradation of methylene blue by these compounds highlights their environmental remediation potentials. The high rate constants and good degradation efficiency within 20 minutes (>90%) demonstrates their suitability for application in wastewater treatment. Hence DETA asymmetric Schiff base complexes offer advantages of stability, visible light absorption, and redox activity, making them promising photo catalysts for dye and pollutant removal [70, 71].

Table 3 Results of Catalytic Degradation of Methylene Blue (MB)

Compds	0 min	4 mins	8 mins	12mins	16 mins	20 mins	R^2	K (min^{-1})
CT	1.242	1.165	1.082	0.998	0.914	0.836	0.9998	0.019
1	1.242	1.081	0.969	0.845	0.733	0.621	0.9961	0.035
5	1.240	1.068	0.919	0.758	0.596	0.460	0.9992	0.049
8	1.241	1.005	0.780	0.563	0.410	0.295	0.9846	0.072
9	1.243	0.910	0.635	0.410	0.270	0.155	0.9627	0.104
10	1.245	0.865	0.575	0.340	0.205	0.110	0.9468	0.115
11	1.244	0.875	0.590	0.355	0.215	0.120	0.9508	0.111

1 = DETA, 2 = Furfural, 4 = Vanillin, 5 = DVF, 6 = Citric acid, 7 = Salicylaldehyde, 8 = $[Mn(DVF)(CA)]Cl_2$, 9 = $[Cu(DVF)(S)]2NO_3$, 10 = $[Fe_2(DVF)_2(Cl)_4]Cl_2$, 11 = $[Cu_2(DVF)_2(NO_3)_2]3H_2O$. 12 = Nystatin, CT = MB+H_2O_2+DMSO

7. Conclusion

The asymmetric Schiff base - DVF and its metal complexes were successfully synthesised and characterised, with spectroscopic and physical data confirming their formation. The Geometry of the compounds could not be determined due to their hygroscopic nature. Biological assays demonstrated strong antibacterial and moderate antifungal activity, with Cu(II) and Fe(III) complexes outperforming controls. Catalytic evaluations confirmed efficient dye degradation via

MLCT and ROS generation. The molecular docking studies highlighted anticancer potentials of the compounds aligning with experimental findings. Collectively, these results position DVF-derived Schiff bases and complexes as multifunctional candidates for AMR drug discovery and environmental remediation, bridging biomedical and industrial applications.

Compliance with ethical standards

Acknowledgments

We acknowledge the valuable contributions of the Department of Chemistry, University of Uyo to the success of this research

Disclosure of conflict of interest

There is no competing interests related to this study.

References

[1] Antimicrobial Resistance Collaborators, "Global burden of bacterial antimicrobial resistance in 2019: a systematic analysis," The Lancet, vol. 399, no. 10325, pp. 629–655, Feb. 2022, doi: 10.1016/S0140-6736(21)02724-0. Antimicrobial Resistance Collaborators. Global burden of bacterial antimicrobial resistance in 2019: a systematic analysis. Lancet. 2022;399(10325):629–55. doi:10.1016/S0140-6736(21)02724-0.

[2] World Health Organization. Antimicrobial resistance. WHO Fact Sheets. 2021. Available from: https://www.who.int/news-room/fact-sheets/detail/antimicrobial-resistance [Accessed 2025 Feb 20].

[3] Munita JM, Arias CA. Mechanisms of antibiotic resistance. Microbiol Spectr. 2016;4(2):1–37. doi:10.1128/microbiolspec.VMBF-0016-2015.

[4] Ventola CL. The antibiotic resistance crisis: part 1: causes and threats. P&T. 2015;40(4):277–83. PMID:25859123; PMCID:PMC4378521.

[5] Belay WY, Getachew M, Tegegne BA, Teffera ZH, Dagne A, Zeleke TK, et al. Mechanism of antibacterial resistance, strategies and next-generation antimicrobials to contain antimicrobial resistance: a review. Front Pharmacol. 2024;15:1444781. doi:10.3389/fphar.2024.1444781.

[6] Bray F, Parkin DM. Cancer in sub-Saharan Africa in 2020: a review of current estimates of the national burden, data gaps, and future needs. Lancet Oncol. 2022;23(6):719–28. doi:10.1016/S1470-2045(22)00270-4.

[7] Islam TM, Bitu NA, Chaki BM, Hossain MJ, Asraf MA, Hossen MF, et al. Water-soluble Schiff base ligands and metal complexes: an overview considering green solvent. RSC Adv. 2024;14(35):25256–72. doi:10.1039/D4RA04310C.

[8] Juyal VK, Pathak A, Panwar M, Thakuri SC, Prakash O, Agrwal A, et al. Schiff base metal complexes as a versatile catalyst: a review. J Organomet Chem. 2023;999:122825. doi:10.1016/j.jorganchem.2023.122825.

[9] Simon N, Ufot IN, Johnson AS, Anweting I, Johnson EC. Synthesis, characterisation, In Silico analysis, and antimicrobial evaluation of mixed-ligand metal (II) complexes of quercetin-8-sulphonic acid and citric acid. Comput Appl Sci Impact. 2025;2(2):16–44. doi:10.1234/casi.v2i2.14.

[10] Ufot IN, Nzikahyel S, Johnson AS, Mkpenie V, Christopher DT, et al. Advances and challenges in diethylenetriamine-based Schiff bases: synthesis, structural diversity, coordination chemistry, and emerging applications. Asian J Chem Sci. 2026;16(2):68–94. ⟨hal-05591986⟩.

[11] Dandapani S, Rossé G, Southall N, Salvino J, Thomas C. Selecting, acquiring, and using small molecule libraries for high-throughput screening. Curr Protoc Chem Biol. 2012;4. doi:10.1002/9780470559277.ch110252.

[12] Fecik RA, Frank K, Gentry E, Mitscher L, Shibata M. Use of combinatorial and multiple parallel synthesis methodologies for the development of anti-infective natural products. Pure Appl Chem. 1999;71:559–64. doi:10.1351/pac199971040559.

[13] Al-Shamry AA, Khalaf MM, El-Lateef HMA, Yousef TA, Mohamed GG, El-Deen KMK, et al. Development of new azomethine metal chelates derived from isatin: DFT and pharmaceutical studies. Materials (Basel). 2022;16(1):83. doi:10.3390/ma16010083.

[14] Kumar M, Singh AK, Gupta J, Singh S, Yadav RK, Singh AP. Exploring mixed-ligand cobalt(II) complexes with salicylaldehyde-based N,O-donor bidentate Schiff bases and neutral N-donor ligands: synthesis, characterization, DFT, and antimicrobial studies. J Indian Chem Soc. 2025;102(8):101803. doi:10.1016/j.jics.2025.101803.

[15] Sharma S, Gupta R, Singh R. Vanillin and its derivatives: Antimicrobial and anti-inflammatory potential. Phytother Res. 2020;34(5):1100–12. doi:10.1002/ptr.6604.

[16] Clark JH, Milescu RA. Furfural as a bio-based platform molecule in industry: Feedstocks and new chemistries. Renew Chem. 2026;2(1):1. doi:10.53941/rc.2026.100001.

[17] Behera G, Sidhanty R, Sutar AK, Maharana T. Schiff bases and their transition metal complexes as cornerstones in applied chemistry. Discov Chem. 2026;3:119. doi:10.1007/s44371-026-00536-5.

[18] Yang J, Shi R, Zhou P, Qiu QM. Asymmetric Schiff bases derived from diaminomaleonitrile and their metal complexes. J Mol Struct. 2015;1106:1. doi:10.1016/j.molstruc.2015.10.092.

[19] Mahar N, Memon AA, Panhwar QK, Afridil HI, Mahar I, Mallah S. Synthesis and antioxidant activity of mixed ligand complex of quercetin and aspartic acid with cobalt(II). Med Chem. 2018;8:253–8. doi:10.4172/2161-0444.1000521.

[20] Raza A, Xu X, Xia L, Xia C, Tang J, Ouyang Z. Quercetin-iron complex: synthesis, characterization, antioxidant, DNA binding, DNA cleavage, and antibacterial activity studies. J Fluoresc. 2016;26(6):2023–31. doi:10.1007/s10895-016-1896-y.

[21] Obaleye J, Tella A, Adesina W, Simon N, Omojasola P. Synthesis, characterization, crystal structure and antimicrobial evaluation of a novel –M–X–M–X– type infinite chain 1D Cu(II) complex with eflornithine hydrochloride hydrate as ligand. J Inorg Organomet Polym Mater. 2014; 24:827–35. doi:10.1007/s10904-014-0052-x.

[22] Zhang X, Zhang G, Yue M, Xue J, Xia S, Ni Z. Photocatalytic degradation of methylene blue by Schiff-base cobalt modified CoCr layered double hydroxides. J Inorg Mater. 2019. doi: 10.15541/jim20180558.

[23] Fasna PHF, Sasi S, Sharmila TKB, Chandra CSJ, Antony JV, Raman V. Photocatalytic remediation of methylene blue using Schiff base-Cu complexes. Environ Sci Pollut Res. 2022; 29:54318–29. doi: 10.1007/s11356-022-19694-x.

[24] Al-Dhahli AS, Al-Hassani FA, Alarjani M. Essential oil from the rhizomes of the Saudi and Chinese Zingiber officinale cultivars: comparison of chemical composition, antibacterial and molecular docking studies. J King Saud Univ Sci. 2020;32:3343–50. doi:10.1016/j.jksus.2020.09.020.

[25] Ufot IN, Nzikahyel S, Johnson AS, Ekarika CJ, Anweting IB, Mkpenie V. Evaluation of the binding affinities of mixed ligands metal (II) complexes of quercetin sulphonic acids on breast cancer cells using molecular docking. Appl Sci Comput Energy. 2025;2(2):353–67. Available from: https://cemrj.com/index.php/volumes/article/view/25.

[26] Jejurikar BL, Rohane SH. Drug designing in Discovery Studio. Asian J Res Chem. 2021;14:135–8. doi:10.5958/0974-4150.2021.00025.0.

[27] Trott O, Olson AJ. AutoDock Vina: Improving the speed and accuracy of docking with a new scoring function, efficient optimization, and multithreading. J Comput Chem. 2010;31(2):455–61. doi:10.1002/jcc.21334.

[28] Fletcher S, Biswas-Fiss EE, Biswas SB. Structural and functional roles of conserved residues of human papillomavirus (HPV) E2 protein and biological consequences. Virol J. 2025. doi:10.1186/s12985-025-02903-7.

[29] Wisniewska M, Bossenmaier B, Georges G, Hesse F, Dangl M, Kunkele KP, et al. The 1.1 Å resolution crystal structure of the p130cas SH3 domain and ramifications for ligand selectivity. J Mol Biol. 2005;347:1005–15. doi:10.1016/j.jmb.2005.02.017. PMID:15784259.

[30] Bohl CE, Wu Z, Miller DD, Bell CE, Dalton JT. Crystal structure of the T877A human androgen receptor ligand-binding domain complexed to cyproterone acetate provides insight for ligand-induced conformational changes and structure-based drug design. J Biol Chem. 2007;282:13648–55. doi:10.1074/jbc.M611711200. PMID:17311914.

[31] Ali I, Wani W. Empirical formulae to molecular structures of metal complexes by molar conductance. Synth React Inorg Met-Org Nano-Met Chem. 2012;43. doi:10.1080/15533174.2012.756898.

[32] Chohan ZH, Supuran CT, Scozzafava A. Metal-based antibacterial agents: Schiff base complexes of transition metals. J Enzyme Inhib Med Chem. 2006;21(2):193–201. doi:10.1080/14756360600623515.

[33] Ajlouni A, Taha ZA, Al-Hassan K, Abu Anzeh AM. Metal complexes of Schiff bases derived from 2-thiophenecarboxaldehyde and mono/diamine as the antibacterial agents. Mod Chem. 2014;2(2). doi:10.11648/J.MC.20140202.11.

[34] Fang F, Li Y, Cui G. Polyamine-derived Schiff bases: Structural features and biological activity. Bioorg Chem. 2019;87:45–55. doi:10.1016/j.bioorg.2019.03.012.

[35] Sharma S, Gupta R, Singh R. Vanillin and its derivatives: Antimicrobial and anti-inflammatory potential. Phytother Res. 2020;34(5):1100–12. doi:10.1002/ptr.6604.

[36] Emara AAA. Structural, spectral and biological studies of binuclear tetradentate metal complexes of N3O Schiff base ligand synthesized from 4,6-diacetylresorcinol and diethylenetriamine. Spectrochim Acta A Mol Biomol Spectrosc. 2010;77(1):117–25. doi:10.1016/j.saa.2010.04.036.

[37] Dag B, Tenekecioğlu Y, Aral T, Kızılkaya H, Erenler R, Genc N. Synthesis, characterization, and antioxidant activity of Schiff base and its metal complexes. Russ J Bioorg Chem. 2023;49(6):861–6. doi:10.1134/S1068162023040106.

[38] Clarke RM, Storr T. The chemistry and applications of multimetallic salen complexes. Dalton Trans. 2014;43(25):9380–91. doi:10.1039/C4DT00591K.

[39] Gvozdev M, Turomsha I, Osipovich N, Sverdlov R, Loginova N. Sterically hindered catechol-derived Schiff bases: SAR and antioxidant mechanisms. RSC Med Chem. 2025. doi:10.1039/D5MD00969C.

[40] Hussain R, Rubab SL, Maryam A, Ashraf T, Arshad M, Lal K, et al. Synthesis, spectroscopic and nonlinear optical properties, and antimicrobial activity of Cu(II), Co(II), and Ni(II) complexes: experimental and theoretical studies. ACS Omega. 2023;8(45):42598–609. doi:10.1021/acsomega.3c05322.

[41] He Y, Huang YY, Zhu XQ, Su SD, Xu QD, Fu JH, et al. Electronic transition and magnetic coupling regulation in trimetallic complexes featuring a new bridging ligand obtained by oxidative addition. Inorg Chem. 2023;62(30):11932–42. doi:10.1021/acs.inorgchem.3c0133.

[42] Chang HN, Li YF, Cui GH, Wang SC. Photocatalytic properties of supramolecular Schiff base complexes. Transit Met Chem. 2017;42:509–15. doi:10.1007/s11243-017-0155-7.

[43] Kargar H, Ardakani AA, Tahir MN, Ashfaq M, Munawar KS. Synthesis, spectral characterization, crystal structure determination and antimicrobial activity of Ni(II), Cu(II) and Zn(II) complexes with the Schiff base ligand derived from 3,5-dibromosalicylaldehyde. J Mol Struct. 2021;1229:129842. doi:10.1016/j.molstruc.2020.129842.

[44] Mohamed GG, Omar MM, Hindy AM. Synthesis, characterization and biological activity of some transition metals with Schiff base derived from 2-thiophene carboxaldehyde and aminobenzoic acid. Spectrochim Acta A Mol Biomol Spectrosc. 2005;62(4–5):1140–50. doi:10.1016/j.saa.2005.03.031.

[45] Ye G, Zhou Z, Wu K, Wang Y, Zong Y, Chen Z, et al. Nitrogen coordination engineering in Co–N4 single-atom catalysts: distinct roles of pyridinic and pyrrolic coordination in regulating reactive oxygen species generation. ACS Catal. 2026;16(4):4053–62. doi:10.1021/acscatal.6c00407.

[46] Uddin MN, Chowdhury DA, Rony MM, Halim ME. Metal complexes of Schiff bases derived from 2-thiophenecarboxaldehyde and mono/diamine as the antibacterial agents. Mod Chem. 2014;2(2):6–14. doi:10.11648/j.mc.2 Al-Hamdani AH, Al-Saadi AA, Al-Khafaji MA, Al-Mousawi SA, Al-Taie HA, Al-Sultani AA. A novel avenue in the successful synthesis of Schiff base macromolecules via innovative plasma and classical approaches. Sci Rep. 2025;15(1):94665. doi:10.1038/s41598-025-94665-z.

[47] Kumar V. Synthesis and characterization of Co(II), Ni(II) and Cu(II) complexes with unsymmetrical tetradentate Schiff base ligand. Res J Chem Environ. 2023;28:82–5. doi:10.25303/282rjce82085.

[48] Palanimurugan M, Kulandaisamy A. Biological screening studies of DNA relate metal complexes from benzylidene-4-imino-2,3-dimethyl-1-phenyl-3-pyrazolin-5-one and 2-aminothiazole. Asian J Chem. 2018;30:594–602. doi:10.14233/ajchem.2018.21042.

[49] Khan S, Muhammad M, Algethami JS, Al-Saidi HM, Almahri A, Hassanian AA. Synthesis, characterization and applications of Schiff base chemosensor for determination of Cr(III) ions. J Fluoresc. 2022;32:1889–98. doi:10.1007/s10895-022-02990-7.

[50] Saravanan C, Ashwin BCMA, Manoj S, Senthilkumaran M, Sethuraman V, Bhargav PB, et al. Schiff base covalent organic polymers as electrode material for supercapacitor application. Mater Lett. 2022;320:132348. doi:10.1016/j.matlet.2022.132348.

[51] Hwang SJ, Kim SK, Lee JG, Lee SC, Jang JH, Kim P, et al. Role of electronic perturbation in stability and activity of Pt-based alloy nanocatalysts for oxygen reduction. J Am Chem Soc. 2012;134(48):19508–11. doi:10.1021/ja307951y.

[52] Boulechfar C, Ferko H. Schiff bases and their metal complexes: A review on the history, synthesis, and applications. Inorg Chem Commun. 2023;150:110451. doi:10.1016/j.inoche.2023.110451.

[53] Charitha R, Kavitha K, Ramya P. Synthesis, characterization and antimicrobial studies of novel Schiff base and its 3d series metal complexes. Indian J Chem A. 2026;65(1):11–7. doi:10.56042/ijc.v65i1.18547.

[54] Nakamoto K. Infrared and Raman Spectra of Inorganic and Coordination Compounds. 6th ed. Hoboken: Wiley; 2008. ISBN:9780470405840.

[55] Abbass LM, Yousif NM, Sadeek SA, Zordok WA, El-Attar MS, El-Farargy AF, et al. Structural characterization, XRD, DFT calculations, docking, antimicrobial, anticancer applications, and electrochemical performance studies of some new Schiff base transition metal complexes. Appl Organomet Chem. 2025;39(4):e70099. doi:10.1002/aoc.70099.

[56] Thakor PM, Patel JD, Patel RJ, Chaki SH, Khimani AJ, Vaidya YH, et al. Exploring new Schiff bases: synthesis, characterization, and multifaceted analysis for biomedical applications. ACS Omega. 2024;9(49):49567–85. doi:10.1021/acsomega.4c02007.

[57] Kumar B, Devi J, Dubey A, Kumar M. Exploration of newly synthesized transition metal (II) complexes for infectious diseases. Future Med Chem. 2024;16(20):2087–105.

[58] Okasha RM, Mohamed AAH, Elhenawy AA, Alshli MH, Alsaedi WH, Alblewi FF, et al. A novel avenue in the successful synthesis of Schiff base macromolecules via innovative plasma and classical approaches. Sci Rep. 2025;15:10840. doi:10.1038/s41598-025-94665-z.

[59] Omar MO, Mahmoud WH, Mamdoh Y, Mohamed GG. Metal complexes of tridentate Schiff base: synthesis, characterization, biological activity and molecular docking studies with COVID-19 protein receptor. Preprint. 2021. doi:10.21203/rs.3.rs-207632/v1.

[60] Sridevi N, Madheswari D. Synthesis, characterization, and biological evaluation of Schiff base ligand and their metal complexes: implications for coordination chemistry and biomedical applications. Polyhedron. 2025;282:117796. doi:10.1016/j.poly.2025.117796.

[61] Claudel M, Schwarte JV, Fromm KM. New antimicrobial strategies based on metal complexes. Chemistry. 2020;2(4):849–99. doi:10.3390/chemistry2040056.

[62] Paterson JR, Beecroft MS, Mulla RS, Osman D, Reeder NL, Caserta JA, et al. Insights into the antibacterial mechanism of action of chelating agents by selective deprivation of iron, manganese, and zinc. Appl Environ Microbiol. 2022;88(2):e0164121. doi:10.1128/AEM.01641-21.

[63] Ali M, Khan MS, Ahmad A. Antifungal potential of Schiff base metal complexes: structure–activity relationship. J Mol Struct. 2019;1180:45–53. doi:10.1016/j.molstruc.2018.11.045.

[64] Dighe SJ, Kamble HV, Ghodake SR. Molecular docking-guided design and synthesis of Schiff base metal complexes as antioxidant and anticancer agents – A review. Int J Pharm Sci. 2025;3(8):2786–91. doi:10.5281/zenodo.16949332.

[65] El-Naggar NE, El-Shall H, Elyamny S, Hamouda RA, Eltarahony M. Novel algae-mediated biosynthesis approach of chitosan nanoparticles using Ulva fasciata extract, process optimization, characterization and their flocculation performance. Int J Biol Macromol. 2024;282(3):136925. doi:10.1016/j.ijbiomac.2024.136925.

[66] Mostafa MA, Ismail MM, Morsy JM, et al. Synthesis, characterization, anticancer, and antioxidant activities of chitosan Schiff bases bearing quinolinone or pyranoquinolinone and their silver nanoparticles derivatives. Polym Bull. 2023;80:4035–57. doi:10.1007/s00289-022-04238-7.

[67] Ouameur AA, Arakawa H, Ahmad R, Naoui M, Tajmir-Riahi HA. A comparative study of Fe(II) and Fe(III) interactions with DNA duplex: major and minor grooves bindings. DNA Cell Biol. 2005;24(6):394–401. doi:10.1089/dna.2005.24.394. PMID:15941392.

[68] Vallavoju R, Kore R, Parikirala R, Subburu M, Gade R, Kumar V, et al. Synthesis and characterization of new tetradentate N2O2-based Schiff's base Cu(II) complexes for dye photodegradation. Photochem. 2023;3(2):274–87. doi:10.3390/photochem3020016.

[69] Jyoti J, An J, Kim D, Churchill DG, Kumar A. Cobalt corroles: synthesis and applications. Coord Chem Rev. 2024;511:215869. doi:10.1016/j.ccr.2024.215869.

[70] Abdelghany MM, Ahmed IS, Dessouki HA, Abdelrahman EA. Facile synthesis of CuO and Ag nanoparticles by thermal decomposition of novel Schiff base complexes. J Inorg Organomet Polym Mater. 2021;31:1–19. doi:10.1007/s10904-021-02032-y.